Accepted Manuscript

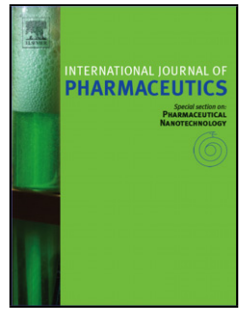


Title: Multifunctional Nanomedicine Platform for Concurrent Delivery of Chemotherapeutic Drugs and Mild Hyperthermia to Ovarian Cancer Cells

Author: Olena Taratula Raj Kumar Dani Canan Schumann Hong Xu Andrew Wang Han Song Pallavi Dhagat Oleh Taratula

| | |
|---|---|
| PII: | S0378-5173(13)00878-8 |
| DOI: | http://dx.doi.org/doi:10.1016/j.ijpharm.2013.09.032 |
| Reference: | IJP 13652 |

To appear in: *International Journal of Pharmaceutics*

| | |
|---|---|
| Received date: | 4-6-2013 |
| Revised date: | 20-8-2013 |
| Accepted date: | 24-9-2013 |

Please cite this article as: Taratula, O., Dani, R.K., Schumann, C., Xu, H., Wang, A., Song, H., Dhagat, P., Taratula, O., Multifunctional Nanomedicine Platform for Concurrent Delivery of Chemotherapeutic Drugs and Mild Hyperthermia to Ovarian Cancer Cells, *International Journal of Pharmaceutics* (2013), http://dx.doi.org/10.1016/j.ijpharm.2013.09.032

# Multifunctional Nanomedicine Platform for Concurrent Delivery of Chemotherapeutic Drugs and Mild Hyperthermia to Ovarian Cancer Cells

**Olena Taratula[a], Raj Kumar Dani[a], Canan Schumann[a], Hong Xu[b], Andrew Wang[b], Han Song[c], Pallavi Dhagat[c], Oleh Taratula[a,]***

[a]Department of Pharmaceutical Sciences, College of Pharmacy, Oregon State University, 1601 SW Jefferson Street, Corvallis, OR 97331, USA

[b]Ocean NanoTech LLC, 700 Research Center Boulevard, Springdale, AR 72764, USA

[c]School of Electrical Engineering and Computer Science, Oregon State University, 1148 Kelley Engineering Center, Corvallis, Oregon 97331

*Address for Correspondence:

**Oleh Taratula, Ph.D.**

Assistant Professor of Pharmaceutical Sciences

Department of Pharmaceutical Sciences

College of Pharmacy

Oregon State University

1601 SW Jefferson Street

Corvallis, Oregon 97331

Phone: +1 541-737-5785

Fax: +1 541-737-3999

E-mail: oleh.taratula@oregonstate.edu

**Abstract (must not exceed 200 words)**

A multifunctional tumor-targeting delivery system was developed and evaluated for an efficient treatment of drug-resistant ovarian cancer by combinatorial therapeutic modality based on chemotherapy and mild hyperthermia. The engineered iron oxide nanoparticle (IONPs)-based nanocarrier served as an efficient delivery vehicle for doxorubicin and provided the ability to heat cancer cells remotely upon exposure to an alternating magnetic field (AMF). The nanocarrier was additionally modified with polyethylene glycol and LHRH peptide to improve its biocompatibility and ability to target tumor cells. The synthesized delivery system has an average size of 97.1 nm and a zeta potential close to zero, both parameters favorable for increased stability in biological media and decreased elimination by the immune system. The nanocarrier demonstrated faster drug release in acidic conditions that mimic the tumor environment. It was also observed that the LHRH targeted delivery system could effectively enter drug resistant ovarian cancer cells, and the fate of doxorubicin was tracked with fluorescence microscope. Mild hyperthermia (40 °C) generated by IONPs under exposure to AMF synergistically increased the cytotoxicity of doxorubicin delivered by the developed nanocarrier to cancer cells. Thus, the developed IONPs-based delivery system has high potential in the effective treatment of ovarian cancer by combinatorial approach.

**Keywords:** Iron oxide nanoparticles; combinatorial treatment; mild hyperthermia; alternating magnetic field (AMF); doxorubicin; ovarian cancer.

## 1. Introduction

Ovarian cancer is a significant cause of cancer death in women worldwide. The high mortality rate is attributed to the fact that ovarian cancer is generally detected at an advanced stage when the tumor has already disseminated at the peritoneal surfaces (Jelovac and Armstrong, 2011; Lengyel, 2012). Because of the distribution of advanced ovarian cancer, micronodular and floating tumor colonies cannot be adequately treated by surgery and require extensive chemotherapy. Although most patients respond effectively to initial chemotherapy, recurrence occurs in up to 75% cases (Jelovac and Armstrong, 2011; Lengyel, 2012). Patients with recurrent ovarian cancer ultimately develop resistance to chemotherapy and are generally incurable (Sehouli et al., 2008). Therefore, there is a critical need to develop novel therapeutic approaches that can improve the efficacy of conventional chemotherapy in drug-resistant ovarian cancer cells. In this regard, combinatorial treatment modalities that simultaneously target different pathways provide a promising direction for overcoming the drug resistance issue and achieving greater therapeutic outcomes (Kleef et al., 2012; Zhang et al., 2012). Moreover, these therapeutic approaches can employ lower doses of anticancer agents in order to avoid undesirable side effects on healthy organs (Zhang et al., 2012).

It was demonstrated that the combination of conventional chemotherapy with mild hyperthermia produces synergistic therapeutic effects on tumor cells and reduces the required effective doses of the anti-cancer drugs (Kleef et al., 2012; Kulshrestha et al., 2012). Mild hyperthermia is an adjuvant therapeutic modality to treat cancer by maintaining the temperature of the tumor region at 40–44 °C (Falk and Issels, 2001; Levi-Polyachenko and Stewart, 2011). At this temperature range, heat increases the efficacy of different chemotherapeutic drugs and combinatorial treatment is much more effective than the each of the two treatments applied separately (Pradhan et al., 2010; Wang et al., 2011). However, a critical barrier faced by both conventional chemotherapy and hyperthermia has been the inability to deliver anticancer drugs and heat to the tumors in a precise manner. Nonspecific delivery leads to undesired side effects to normal organs and tissues, and lowers the dosages of heat and anticancer drugs at tumor sites required to kill cancer cells. Therefore, if both heat and chemotherapeutic drugs can be selectively and concurrently delivered to the tumorigenic region, the therapeutic efficacy of the combinatorial treatment is expected to be significantly improved with minimal side effects. Recent studies have demonstrated the possibility for concurrent delivery of chemotherapy and hyperthermia by the nanoparticles-based delivery systems (Kulshrestha et al., 2012; Wang et al., 2011). In particular, magnetic iron oxide nanoparticles (IONPs) offer a great potential as they can be loaded with anticancer agents and remotely heated with an external alternating magnetic field (AFM) after localization in cancer tumors (Lee et al., 2011; Pradhan et al., 2010). Moreover, there is an opportunity to modify IONPs-based delivery systems with cancer cell targeting moieties in order to improve tumor targeted localization (Fan et al., 2011; Taratula et al., 2011b; Yu et al., 2012a). There are a number of reports describing the successful development of water soluble iron oxide nanoparticles for anticancer drug delivery and imaging (Ahmd et al., 2012; Ahsan et al., 2013).

The most widely studied approach to prepare the IONPs-based delivery system for combinatorial treatment is based on co-encapsulation of both chemotherapeutic drugs and iron oxide nanoparticles within liposomes, resulting in so called magnetoliposomes. Thus, several recent reports discuss the preparation and application of magnetoliposomes containing different chemotherapeutic agents for combinatorial treatment of cancer cells *in vitro* (Kulshrestha et al., 2012; Pradhan et al., 2010; Wang et al., 2011). For instance, Pradhan et al. successfully synthesized folate-targeted magnetoliposomes containing doxorubicin (DOX), which demonstrated significant improvement in cancer cell treatment in comparison to drug loaded non-magnetic liposomes (Pradhan et al., 2010). Although these approaches have shown favorable results on cultured cancer cells, the resulted magnetoliposomes tend to be large (>300 nm) in size and may have limited application for systemic delivery *in vivo*. A major obstacle for systemic delivery of large delivery systems is that the reticuloendothelial system (RES) detects and phagocytosis them, preventing their targeting and therapeutic action. In general, drug delivery systems that are 10–100 nm in size are considered to be optimal for systemic delivery whereas particles >200 nm and <10 nm are sequestered by the spleen or removed through renal clearance, respectively (Alexis et al., 2008; Longmire et al., 2008). Moreover, the current size of magnetoliposomes would probably be too large to exploit the enhanced permeability and retention (EPR) effect for targeting delivery systems to invade cancer tumors. Thus, only liposomes of an average size of approximately 200 nm or less are optimal for the EPR effect and have a significant chance of encountering the leaky vessels of tumor tissue (Maruyama, 2011).

In order to overcome the above mentioned barriers, down-sizing of the formulated magnetoliposomes is required. However, this step may result in lower encapsulation efficiency of iron oxide nanoparticles, which compromises the ability of magnetoliposomes to function as an efficient hyperthermia source. In addition, while doxorubicin encapsulation within magnetoliposomes was reported to be relatively high, there is certainly a need to further optimize magnetic particle incorporation (Pradhan et al., 2010). However, an increase in IONPs loading may lead to even larger magnetoliposomes.

In this work, we created a novel tumor targeted delivery system for combinatorial treatment of drug resistant ovarian cancer cells. The synthesized delivery system has an average size of 97.1 nm and a zeta potential close to zero, both parameters being favorable for increased stability in biological media and decreased elimination by the immune system. In order to achieve this, we synthesized superparamagnetic IONPs with a hydrodynamic diameter of 70.8 nm containing magnetic iron oxide nanocrystals surrounded by three polymer layers (Fig. 1). Due the presence of a polymer shell, each nanoparticle can be efficiently loaded with DOX and exhibit triggered drug release in acidic conditions that mimic the cancer tumor environment (Fig. 1A). To enhance steric stability and extend blood circulation of the delivery system (Alexis et al., 2008; Taratula et al., 2009), the surface of the drug loaded IONPs was modified with heterobifunctional polyethylene glycol (PEG) layer (Fig. 1B). Finally, Luteinizing Hormone-Releasing Hormone (LHRH) peptide, as a ligand to LHRH receptors in human ovarian cancer cells (Taratula et al., 2009; Zhang et al., 2012), was conjugated to the distal end of PEG for delivery system targeting specifically to the cancer tumor (Fig. 1C). The developed delivery system efficiently generates heat in the presence of AMF and synergistically increases cytotoxicity of the delivered DOX in drug resistant ovarian cancer cells.

## 2. Materials and methods

### 2.1 Materials

Oleic acid, 1-octadecene, Poly (Maleic Anhydride-*alt*-1-Octadecene) (PMAO, MW=30,000–50,000 Da), Poly(ethyleneimine) (PEI, MW 25,000 Da), microsized iron (III) oxide, were obtained from Sigma-Aldrich and used without further purification. Doxorubicin hydrochloride (DOX) was purchased from Polymed Therapeutics (Houston, TX). $\alpha$-Maleimide-$\omega$-N-hydroxysuccinimide ester polyethylene glycol (MAL-PEG-NHS) was obtained from NOF Corporation (White Plains, NY). A synthetic analog of LHRH, Lys6–des-Gly10–Pro9-ethylamide (Gln–His–Trp–Ser–Tyr–DLys(DCys)–Leu–Arg–Pro–NH–Et) peptide was synthesized by Amersham Peptide Co. (Sunnyvale, CA). Trinitrobenzene sulfonic acid (TNBSA) and Bicinchoninic Acid (BCA) protein assay kit were obtained from Pierce (Rockford, IL). All other chemicals were purchased from VWR (Visalia, CA).

## 2.2 Preparation of the delivery system

### 2.2.1 Iron oxide nanoparticles synthesis

IONPs were prepared using iron oxide powder as the iron precursor, oleic acid as the ligands, and 1-octadecene as the solvent according to the previously described procedure (Taratula et al., 2011b; Yang et al., 2008). Briefly, iron oxide nanocrystals were synthesized in organic solvents at a high temperature. Typically, microsized iron oxide was mixed with oleic acid, 1-octadecene, and then heated to 320 ºC to produce monodisperse (5–10% size distribution) iron oxide nanocrystals. The size of the nanoparticles was controlled by reaction time, temperature, and the iron oxide and oleic acid concentrations. After the reaction was completed, the mixture was cooled and the iron oxide nanocrystals were precipitated out of 1-octadecene by chloroform/acetone, and then redispersed in chloroform. These nanocrystals were highly crystalline and uniform but were not dispersible in water due to the hydrophobic oleic acid capping layer. For dispersion of iron oxide nanoparticles in water, we modified a previously published method based on forming micelles through amphiphilic polymer (PMAO) for transferring iron oxide nanocrystals from organic solvents into water (Yang et al., 2009; Yu et al., 2006). Prior modification of iron oxide nanocrystals, PMAO was hydrolyzed at 80 °C in 0.5 M NaOH for 24 hrs. The hydrophobic part of this polymer has 18-carbon alkaline side residues that intercalate and interact hydrophobically with the oleic acid chains that cover the iron oxide core. The hydrophilic part of the polymer, the carboxylic groups, is exposed to the outermost part of the nanoparticles conferring stability to them (Moros et al., 2010). PMAO modified iron oxide nanoparticles were added to PEI aqueous solution and the PEI was allowed to adsorb for 20 min under stirring. The formed nanoparticles were purified by ultracentrifugation and used for further studies.

2.2.2 Drug loading into iron oxide nanoparticles

Drug loading was achieved by simply mixing DOX and IONPs solutions as previously described (Fig. 1A) (Yang et al., 2008). DOX was dissolved in water and then added to the IONPs aqueous solutions at the following weight ratios of DOX to IONPs (iron (Fe) content): (a) 1:1, (b) 1:5 and (c) 1:10. After rotating at room temperature for 12 hrs, free DOX was separated from the encapsulated drug using the Microsep 50 k centrifugal device. The following weight ratios of DOX to IONPs (iron (Fe) content): (a) 1:1 and (b) 1:10 were further employed for cytotoxicity study and combinatorial treatment experiment, respectively. The amount of DOX encapsulated into the IONPs was quantified based on UV-visible absorption spectra of IONPs-DOX samples, with a prominent DOX peak appearing around 460 nm over the IONPs background (UV-1800 spectrophotometer, Shimadzu, Carlsbad, CA). The standard curve was generated by measuring drug absorption intensity at 460 nm in the standard samples containing different concentrations of DOX while using a constant concentration of IONPs (Fe content). Drug loading capacity of IONPs is expressed as the percentage of DOX weight encapsulated into IONPs over the weight of IONPs (Fe content) (Gou et al., 2010). In addition, drug encapsulation efficiency is represented as the percentage of DOX weight encapsulated into IONPs over the total weight of DOX used for drug loading procedure (Gou et al., 2010). The DOX loaded particles will be further mentioned as IONPs-DOX.

### 2.2.3 Modification of IONPs-DOX with PEG and LHRH

The previously published procedure was employed to modify both drug free (IONPs) and DOX loaded IONPs (IONPs-DOX) with PEG and LHRH (Taratula et al., 2009; Taratula et al., 2011b). Briefly, the NHS groups on the distal end of heterobifunctional 5 kDa PEG polymer (MAL-PEG-NHS) were reacted with primary amines on the surfaces of IONPs in 50 mM Phosphate Buffered Saline (PBS) buffer (pH 7.4) at primary amines to PEG molar ratio of 1:2.5 (Fig. 1B). The reaction was carried out for 1 hr at room temperature under shaking, following the addition of LHRH peptide, and then incubation overnight. The molar ratio of MAL-PEG-NHS to LHRH peptide in the reaction mixture was 1:2. The peptide was covalently conjugated to the distal end of PEG layer through the maleimide groups on the PEG and the thiol groups in LHRH (Fig. 1C). After 12 hrs of the reaction, the modified nanoparticles were purified by using Microsep 50 k centrifugal device. The concentration of amino groups available on the IONPs surface before PEGylation as well as the decrease in their concentration after the surface modification was determined by a modified spectrophotometric TNBSA assay as described in our previous report (Taratula et al., 2009). Determination of the presence of LHRH peptide on the surface of either IONPs modified with PEG and LHRH peptide (IONPs-PEG-LHRH) or DOX-loaded IONPs modified with PEG and LHRH peptide (IONPs-DOX-PEG-LHRH) was performed using Bicinchoninic Acid (BCA) protein assay (Pierce, Rockford, IL) as previously described (Taratula et al., 2009; Taratula et al., 2011b). The size, morphology and zeta potential of the developed drug delivery system were evaluated by Transmission electron microscopy (TEM) and Dynamic Light scattering (DLS) (see details in Supplementary data).

## 2.3 Characterization of the delivery system

2.3.1 Drug release study

The drug release profile of DOX from IONPs-DOX-PEG-LHRH was evaluated in PBS at pH 5.5 and 7.4 and 50% human plasma. The drug loaded delivery system was dissolved either in 50% human plasma or in PBS buffer of appropriate pH and placed in a Float-A-Lyzer dialysis tubes (molecular weight cutoff of 50 kDa). The dialysis tubes were immersed in 40 mL of the appropriate solution and incubated at a constant temperature of 37 °C. At fixed time intervals, 200 microliters of the samples were withdrawn from the dialysis tubes to record the absorbance of DOX at 460 nm as described above. After each absorption measurement, the samples were returned to the appropriate dialysis tubes for further incubation. The DOX content in the delivery system at different time points was quantified by using the same approach described above for the drug loading study. The percentage of drug release at different environments and time points was calculated as follows:

$$\text{Drug release (\%)} = [DOX]_R/[DOX]_T \times 100,$$

where $[DOX]_R$ is the amount of DOX released at collection time t and $[DOX]_T$ is the total amount of DOX that was encapsulated in the delivery system.

2.3.2 Specific absorption rate measurements

Specific absorption rate (SAR) determines the heating ability of magnetic materials in the presence of an alternating magnetic field (AMF) and can be defined as the amount of heat generated per unit gram of magnetic material per unit time (Fortin et al., 2007). To measure the SAR values of IONPs alone and IONPs-DOX-PEG-LHRH, 100 μL of each sample (Fe concentration 0.85 mg/mL) was transferred into a standard 0.5 mL microcentrifuge tube and inserted into the insulating sample holder. The sample holder was then placed in the center of a 5-turn cooper coil (40 mm inner diameter), connected to a radio frequency (RF) generator (MSI automation, Wichita, KS) that produces AMF with a constant frequency of 393 kHz and an amplitude of up to 33.5 kA/m. To minimize the influence of heat rising near the coil on the samples, the coil was cooled with circulating cold water. Within the coil, a jacket, through which polypropylene based coolant was circulated, additionally provided a thermal barrier to heat generated directly by the coil. The coolant temperature was adjusted in order to obtain an equilibrium temperature of 25 °C for all the samples prior to AMF application. The samples were then exposed to AMF of 33.5 kA/m amplitude and the temperature rise was recorded in 1-s intervals with a fiber optic probe (Neoptix Inc., QC, Canada) placed in the center of the sample solution. The SAR values of IONPs and IONPs-DOX-PEG-LHRH were determined from the initial slope of the time–temperature curve (dT/dt), as described previously (Fortin et al., 2007). SAR was calculated using the following equation:

$$\mathrm{SAR} = (CV_s/m) \times (\mathrm{d}T/\mathrm{d}t),$$

where $C$ is the specific heat capacity of the medium ($C_{\mathrm{water}} = 4.185$ J g$^{-1}$ °C$^{-1}$), $Vs$ is the sample volume, $m$ is the mass of iron in the sample and d$T$/d$t$ is the initial slope of the time-dependent temperature curve.

## 2.4 *In vitro* study

### 2.4.1 Cell line

The A2780/AD multidrug resistant human ovarian carcinoma cell line was obtained from T. C. Hamilton (Fox Chase Cancer Center, Philadelphia, PA). Cells were cultured in RPMI 1640 medium (Sigma, St. Louis, MO) supplemented with 10% fetal bovine serum (VWR, Visalia, CA) and 1.2 mL/100 mL penicillin–streptomycin (Sigma, St. Louis, MO). Cells were grown at 37 °C in a humidified atmosphere of 5% CO2 (v/v) in air. All experiments were performed on cells in the exponential growth phase.

2.4.2 Cytotoxicity study

The cellular cytotoxicity of all studied formulations was assessed using a modified Calcein AM cell viability assay (Fisher Scientific Inc.). Briefly, cancer cells were seeded into 96-well microtiter plates at the density of 10 x $10^3$ cells/well and allowed to grow for 24 hrs at 37 °C. Then the culture medium was discarded and the cells were treated for 24 hrs with 200 μL of medium containing different concentrations of the following formulations: (1) control (fresh media), (2) IONPs (Fe content from 100 μg/mL to 0.78 μg/mL), (3) IONPs-PEG-LHRH (Fe content from 100 μg/mL to 0.78 μg/mL), (4) free DOX (drug concentration from 15 μg/mL to 0.058 μg/mL), and (5) IONPs-DOX-PEG-LHRH (DOX concentration from 15 μg/mL to 0.058 μg/mL). After treatment, the cells were rinsed with Dulbecco's Phosphate-Buffered Saline (DPBS) buffer and incubated for 1 hr with 200 μL of freshly prepared Calcein AM solution (10 μM in DPBS buffer). Fluorescence was measured using a multiwell plate reader (Synergy HT, BioTek Instruments, Winooski, VT) with a 485 nm excitation and a 528 nm emission filters. On the basis of these measurements, cellular viability was calculated for each concentration of the formulation tested. The 50% inhibitory concentration ($IC_{50}$) was determined as the drug concentration that resulted in a 50% reduction in cell viability.

2.4.3 Cellular internalization

Prior to the visualization, A2780/AD cells were plated in 6-well tissue culture plate at the density of 10 x $10^3$ cells/well and cultured for 24 hrs. The medium was then replaced by a suspension of

(1) IONPs-DOX, (2) IONPs-DOX-PEG, and (3) IONPs-DOX-PEG-LHRH in the culture media at the concentration of doxorubicin of 5 μg/mL and the cells were incubated with the studied formulations for 10 hrs. In addition, to visualize the intracellular accumulations of DOX at different time points, A2780/AD cells were incubated with (1) free DOX and (2) IONPs-DOX-PEG-LHRH for 3 and 24 hrs and their nuclei were stained with 4', 6-diamidino-2-phenylindole (DAPI) for 30 min at 37 °C as previously described (Taratula et al., 2011a). Cellular internalization of the studied formulations was analyzed by a fluorescence microscope (Leica Microsystems Inc., Buffalo Grove, IL).

2.4.4 Quantification of intracellular iron content

The ferrozine-based colorimetric assay was used to estimate the intracellular iron (Fe) content in A2780/AD cells after treatment with the developed delivery system as previously reported (see details in Supplementary data) (Basel et al., 2012).

2.4.5 *In vitro* evaluation of hyperthermia and combinatorial treatment

Prior evaluation of the developed delivery system for hyperthermia applications, A2780/AD cells were plated in T-25 cell culture flasks and grown to 80% of confluence. Subsequently, cells were incubated for 12 hrs with drug free delivery system (IONPs-PEG-LHRH) dispersed in 6 mL of cell culture media (15 μg Fe/mL). Cells loaded with the delivery system were washed with DPBS in order to remove loose IONPs-PEG-LHRH, detached by using 0.25% trypsin/EDTA and resuspended in cell culture media prior to counting. Subsequent to counting, a portion of the cell suspension containing 5 x $10^6$ cells was centrifuged at 1000 rpm for 5 min to form the cell pellet. The formed cell pellets were maintained in a constant volume of 0.1 mL of culture media in a standard 0.5 mL microcentrifuge tube before and during treatment. Samples were then positioned in the center of a 5-turn cooper coil as described above for the SAR evaluation experiment. The water jacket inside of the copper coil was maintained at 37 °C, and the samples were allowed to equilibrate to this temperature before exposure to AMF. The cell pellets were exposed to AMF at fixed 393 kHz frequency and the temperature changes were measured in 1-s intervals by placing a fiber optic temperature probe (Neoptix Inc., QC, Canada) inside of the pellets. Once the cell pellets reached the targeted temperatures (40 °C or 44 °C), the power of the RF generator was adjusted in order to maintain these temperatures for 30 min. After AMF exposure, the cells were cooled to 37 °C, washed with DPBS buffer, resuspended in media and seeded in a 96-well plate at a density of 10 x $10^3$ cells/well and were cultured for another 48 hrs. Finally, the cell viability was assessed using a modified Calcein AM assay as described earlier for the cytotoxicity study.

In addition, three control groups were employed in the current study to evaluate efficacy of hyperthermia and combinatorial treatments. These controls were (1) untreated cells, (2) cells treated with IONPs-PEG-LHRH only and (3) untreated cells exposed to AMF only. Thus, pellets consisting of (1) untreated cells and (2) cells treated with IONPs-PEG-LHRH were placed in the copper coil, allowed to equilibrate to 37 °C using heat generated by the water jacket and maintained under these conditions for 30 min with AMF power off. Finally, for magnetic field only treatments, the pellets of untreated cells were exposed to AMF at the maximum strength for 30 min. The cells from all the control groups were further cultured and evaluated with the cell viability assay as described above.

The cells were treated in the same manner for the chemotherapy only and combinatorial treatment modality (chemotherapy and 30 min of hyperthermia at 40 °C), except that cells in T-25 flask were incubated with the drug loaded delivery system (IONPs-DOX-PEG-LHRH, 1.0 μg DOX/mL and 15 μg Fe/mL) for 12 hrs. Finally, the cell pellets designated to combinatorial treatment experiment were additionally exposed to AMF in order to generate temperature of 40 °C for a 30 min period.

The combined effect of the combinatorial treatment was evaluated by Valeriote's method as described previously (Pradhan et al., 2010). With (A), (B) and (A+B) representing the percentage of cell viability for treatments A (hyperthermia) and B (chemotherapy) and A+B (combinatorial treatment). Combined effects were defined as follows: synergistic, (A+B)<(A)×(B)/100; additive, (A+B)=(A)×(B)/100; sub-additive, (A)×(B)/100<(A+B)<(A), if (A)<(B), interference, (A)<(A+B)<(B), if (A)<(B), antagonistic, (B)<(A+B), if (A)<(B).

### 2.5 Statistical analysis

Data were analyzed using descriptive statistics, single-factor analysis of variance (ANOVA), and presented as mean values ± standard deviation (SD) from three to eight independent measurements. The comparison among groups was performed by the independent sample student's *t*-test. The difference between variants was considered significant if $P < 0.05$.

## 3. Results and discussion

### 3.1 Preparation and characterization of iron oxide nanoparticles

In order to develop the tumor-targeted delivery system for concurrent delivery of chemotherapeutic drugs and nanoheaters, water soluble IONPs covered with three polymer layers such as oleic acid, PMAO and PEI (Fig. 1A) have been synthesized according to the previously published procedure (Taratula et al., 2011b; Yang et al., 2008). The prepared IONPs contain spherical iron oxide cores of 28.5 nm in diameter with relatively uniform size distribution (Fig. 2A and Fig. S1A). The as-synthesized iron oxide cores were hydrophobic owing to an oleate coating. To provide water solubility, oleic acid coated iron oxide crystals were modified with two polymers in tandem such as the monolayers of amphiphilic PMAO and hydrophilic PEI. The prepared IONPs are very stable in most buffer solutions in the pH range of 5-10 and can survive autoclaving process (121 °C for 30 min). Analysis of negatively stained TEM images revealed that the developed nanoparticles with three polymer layers had a diameter of 34.2 ± 2.1 nm and the thickness of polymer layers around the iron oxide cores was approximately 3.5 nm (Fig. 2 A, B and Table 1). Concurrently, the DLS study demonstrated that a hydrodynamic size of the same IONPs nanoparticles was 70.8 ± 0.2 nm (Table 1, Fig. S2A), which is about 35 nm larger than the IONPs diameter measured by TEM. The observed discrepancy between TEM and DLS measurements is not related to the aggregation of the nanoparticles in solution. Thus, a low polydispersity index (PDI) of 0.141 ± 0.010, obtained from DLS measurement, indicates stability and a narrow size distribution of IONPs in solution. Moreover, TEM images further confirmed the presence of non-aggregated nanoparticles with relatively uniform size distribution (Fig. 2A and C). The discrepancy between the obtained results is related to the fact that TEM and DLS are different techniques and TEM provides more accurate size measurement.  It worth mentioning that DLS yields a larger average size by measuring the hydrodynamic diameter of the particle including the solvation layers, while the polymer layers around the iron core could potentially dehydrate and shrink during TEM sample preparation resulting in lower nanoparticle diameter. The zeta potential of the prepared IONPs was highly positive +38.0 ± 1.8mV, which is attributed to the presence of protonated amine groups in the structure of PEI monolayer (Table 1). The TNBSA assay further demonstrated that 1 mg of iron oxide nanoparticles (Fe content) contain 5.4 μmole of primary amine groups, which could be employed for further modification of the developed IONPs with PEG and cell targeting peptide. Furthermore, the presence of the PEI layer on IONPs surface provides a mechanism for the developed delivery system to escape the endosome/lysosome through the proton sponge effect (Yezhelyev et al., 2008). Finally, the magnetic property of the developed IONPs was investigated using a vibrating sample magnetometer at room temperature. The results revealed that the coercivity for IONPs was close to zero, indicating that most particles have superparamagnetic behavior (Fig. S2B) (Lee et al., 2011).

### 3.2 Drug loading

Encapsulation of DOX into iron oxide nanoparticles offers a chance to alter the pharmacokinetics and tissue distribution profile in favor of tumor specific accumulation, and thus minimize cytotoxicity of the chemotherapeutic agent to the healthy organs (Peng et al., 2008). Moreover, several reports indicated that encapsulating drugs into iron oxide nanoparticles is also a promising way for overcoming multidrug resistance (Kievit et al., 2011). Two main strategies to incorporate DOX into iron oxide nanoparticles have been widely employed: (1) conjugation of the drug to the nanoparticles surface via labile chemical bonds (Yang et al., 2010) and (2) physical loading of DOX in the polymer surface layer (Quan et al., 2011; Yang et al., 2008). Because DOX may lose therapeutic efficacy in a conjugated form, the loading of anticancer agent through covalent binding could be a limited approach. Therefore, our drug loading strategy takes advantage of the availability of a drug reservoir formed by three polymer layers on the developed IONPs surfaces. We found that DOX can be efficiently incorporated into the polymer layers on IONPs surfaces by simply mixing the IONPs with the appropriate amount of the drug.

Thus, both drug loading capacity and drug encapsulation efficiency at a DOX to IONPs (Fe) ratio of 1 mg DOX: 1 mg of Fe were equal to 38.0% w/w, respectively. In addition, the loaded drug amount achieved at the above mentioned DOX to IONPs (Fe) ratio was evaluated to be

0.538 mmol per 1 g of IONPs-PEG-LHRH. Moreover, we also demonstrated an ability to control drug loading capacity by changing a DOX to IONPs weight ratio. For instance, a DOX to IONPs ratio of 0.1 mg DOX: 1 mg of Fe decreased drug loading capacity to 6.6% w/w. In general, drug loading capacity showed a strong dependence on DOX concentration during the drug loading process and decreases as the DOX: IONPs ratio is reduced (Fig. S3A). These data revealed a fact that doses of both chemotherapeutic drugs and IONPs can be controlled during concurrent delivery to the cancer cells by the developed delivery system in order to achieve the desired therapeutic outcome. Further, we examined the hydrodynamic size and zeta potential of the DOX loaded IONPs (Table 1). Our result demonstrated that the resulting iron oxide nanoparticles loaded with DOX are 86.4 ± 0.7 nm in diameter with uniform size distribution (PDI 0.129 ± 0.012), which is larger than IONPs alone (70.8 ± 0.2 nm, Table 1 and Fig. S2A). TEM analysis further confirmed an increase in diameter of the DOX loaded nanoparticles (37.5 ± 2.1 nm, Table 1 and Fig. S1B) in comparison to non-modified IONPs (34.2 ± 2.1 nm, Table 1 and Fig. 2B). An increase in the size of nanoparticles can be attributed to the swelling of the polymer coating on the surface of the nanoparticles upon DOX encapsulation. The observed result is in a good agreement with previous studies that demonstrated that the size of human serum albumin coated iron oxide nanoparticles increased by about 20 nm after DOX encapsulation (Quan et al., 2011). In contrast, the zeta potential values of the prepared IONPs (+38.0 ± 1.8) were not affected by the encapsulation of DOX (+42.6 ± 0.7, Table 1). These data indicate that DOX is not physically adsorbed on IONPs and rather encapsulated into the polymer coating of iron oxide nanoparticles.

### 3.3 Development and characterization of targeted delivery system

The size and surface charge are important physiochemical parameters in the development of nanoparticles-based delivery systems. Thus, the positive charge on the surface promotes nanoparticles aggregation in the blood stream, due to electrostatic association with negatively charged serum proteins and results in rapid uptake of drug carriers by the reticuloendothelial system (Alexis et al., 2008). Moreover, positively charged nanoparticles are more toxic than neutral counterparts due to more pronounced disruption of cellular membrane integrity (Taratula et al., 2009). To reduce nonspecific binding with blood components and minimize cytotoxicity due to the presence of positively charged amines groups, DOX loaded IONPs were PEGylated using an excess of heterobifunctional PEG polymer (MAL-PEG-NHS) (Fig. 1B). The employed 5 kDa PEG contains an amine reactive NHS ester and thiol reactive maleimide (MAL) group on the opposite sides and allows for a further modification of IONPs in a layer-by-layer fashion. The PEGylation of IONPs-DOX was carried out by the coupling of linear MAL-PEG-NHS to the amino groups on surface of nanoparticles, introduced by PEI polymer. The availability of the primary amines on the IONPs before PEGylation as well as the decrease in their concentration after modification has been estimated by the TNBSA assay. Thus the obtained data reveal a 95% decrease of $NH_2$ concentration on the surface of the nanoparticles after PEGylation. Moreover, conjugation of heterobifunctional PEG to the positively charged primary amine groups on the DOX loaded IONPs surface resulted in the reduction of zeta potential from +42.6 ± 0.7 mV to +4.9 ± 0.9 mV (Table 1). As was expected, PEGylation significantly minimized the cytotoxicity of the drug free IONPs (Fig. S3B). Thus, the modified drug free nanoparticles do not significantly compromise viability of A2780/AD multidrug resistant human ovarian carcinoma cells in the studied concentration range of 0.8-100 μg/mL (Fig.5A and Fig. S3B), indicating biocompatibility of the developed drug delivery system. On the other hand, non-modified iron oxide nanoparticles reduced viability of the cells more than 50% at the concentrations higher than 50 μg/mL (Fig. S3B). Furthermore, positively charged iron oxide nanoparticles showed strong aggregation in the cell medium containing 10% of fetal bovine serum (Fig. 3A). In the case of the PEGylated nanoparticles, there was no aggregation observed in the serum-supplemented medium (Fig. 3C and E), indicating that the PEG layer can prevent aggregation of the delivery system induced by serum proteins. In order to confirm the obtained result, both non-modified (IONPs-DOX) and PEGylated delivery systems (IONPs-DOX-PEG-LHRH) were dispersed in 50% human plasma and incubated at 37 °C for 24 hrs. The obtained data revealed that PEGylation significantly improved stability of DOX-loaded IONPs nanoparticles in human plasma. Thus the hydrodynamic diameter of non-modified delivery systems (IONPs-DOX) recorded 24 hrs after incubation was significantly increased from 70.8 ± 0.2 nm to 1488.0 ± 38.0 nm, while the size of PEGylated IONPs changed only from 97.1 ± 1.0 nm to 118.9 ± 0.7 nm, respectively (Fig. S4). The tendency of non-modified particles to form aggregates might be attributed to stronger electrostatic interaction between plasma proteins and IONPs which have higher surface charges (+42.6 ± 0.7 mV) as compared to PEGylated drug delivery systems (+4.9 ± 0.9 mV). Another key issue in the development of drug delivery systems is the rapid elimination of nanoparticles from the blood stream, which is attributed to their recognition by macrophages of the mononuclear phagocyte system. Therefore, the uptake of nanoparticles by murine macrophages (RAW264.7) was investigated with the aim of evaluating the capability of nanoparticles to reduce phagocytosis. The intracellular iron content measurement indicated that the uptake of PEG-modified nanoparticles (0.54 pg/cell) into macrophage cells was three times lower than that of unmodified nanoparticles (1.62 pg/cell, Fig. S5). The obtained result is consistent with an earlier report indicating that PEGylation prevents the nanoparticles from agglomeration and increases their resistance to protein adsorption (Zhang et al., 2002).

According to the previous reports, while improving stability and reducing cytotoxicity PEGylation usually limits cellular internalization of the nanoparticle-based delivery systems (Taratula et al., 2009). Thus, the neutral surface charge of PEGylated drug delivery systems reduces their interactions with a negatively charged cell membrane when compared with a positively charged non-modified delivery system (Taratula et al., 2009). Fluorescence microscopy studies revealed that, despite strong aggregations, the non-modified IONPs-DOX were still capable of delivering DOX into A2780/AD human cancer cells (Fig. 3A and B). In contrast, the PEGylated IONPs-DOX showed significantly lower internalization efficiency by the cells under the same experimental conditions (Fig. 3C and D). According to the cell uptake study (Fig. S6), non-modified nanoparticles (IONPs-DOX) were internalized in A2780/AD cells four times more efficiently than their PEGylated counterparts. In general, this positive feature of the surface modification results in the minimization of non-specific cellular internalization and thus reducing side effects of the delivery systems on healthy organs (Taratula et al., 2009). To achieve targeted delivery to the cancer cells and enhance cellular internalization, the modification of sterically stabilized carriers with cell targeting ligands is usually used (Pradhan et al., 2010; Taratula et al., 2009; Zhang et al., 2012). Recently, we successfully employed a modified peptide synthetic analog of LHRH decapeptide as a targeting moiety to tumors overexpressing LHRH receptors, including ovarian cancer tumors (Taratula et al., 2009; Zhang et al., 2012). In order to conjugate a targeting moiety (LHRH peptide) to the IONPs-based delivery system, the maleimide group at the distal end of the PEG-chain was coupled to the thiol group presented by cysteine residue in the modified LHRH sequence. The presence of the LHRH peptide on the complex surface was confirmed by BCA protein assay according to the manufacturer's protocol. Thus, results of fluorescence microscopy and cell uptake studies demonstrated an increase in the cellular internalization of the LHRH targeted delivery systems as compared to PEGylated ones without LHRH targeting moieties (Fig. 3D, F and Fig. S6). Thus, IONPs-DOX-PEG-LHRH were taken up three times more efficiently than IONPs-DOX-PEG in A2780/AD cells. To verify the specific targeting of the LHRH receptor by IONPs-DOX-PEG-LHRH, A2780/AD cells were pre-incubated with the free LHRH peptide prior to the cell uptake study. The obtained result revealed that IONPs-DOX-PEG-LHRH were internalized in the cells two times less efficiently than under normal conditions (without cell pre-incubation and with free LHRH), indicating that the interaction between the LHRH-modified delivery system and cancer cells was competitively inhibited by free LHRH in culture medium. Finally, the hydrodynamic size of the resulting LHRH-PEG-DOX-IONPs was evaluated to be 97.1 ± 1.0 nm (PDI 0.218 ± 0.037), which is larger than DOX-IONPs alone (86.4 ± 0.7 nm, Table 1 and Fig.S2A). Moreover, TEM analysis also demonstrated an increase in diameter of the LHRH-targeted delivery system (43.5 ± 2.8 nm) in comparison to non-modified DOX-loaded nanoparticles (37.5 ± 2.1 nm, Table 1 and Fig. 2C and D). The increase in the size of the DOX loaded IONPs after modification could be explained by the presence of the PEG layer and LHRH peptides on the surface of the delivery system as previously demonstrated (Taratula et al., 2009). According to the previous study by Yu et al, the size of PEGylated iron oxide nanoparticles is a stronger determinant of non-specific uptake by macrophages (Yu et al., 2012b). Thus, the final delivery systems have a hydrodynamic size within the range of 10-100 nm to reduce elimination by the kidneys (<10 nm) and recognition by macrophages cells (>100nm) (Alexis et al., 2008; Longmire et al., 2008).

### 3.4 Intracellular DOX localization and anticancer effect

The intracellular localization of DOX plays an important role in its anticancer activity (MacKay et al., 2009; Shi et al., 2009). Therefore, localization of DOX in the A2780/AD ovarian carcinoma cells after incubation with either free drug or drug loaded into LHRH targeted IONPs was evaluated by fluorescence microscopy. We found that initially DOX delivered by IONPs was predominantly distributed in the cytoplasm after 3 hrs of incubation (Fig. 4A and B), but later also diffused in the cell nuclei (Fig. 4C and D), where it is expected to exert a therapeutic effect. In contrast, free DOX incubated with A2780/AD cells was only localized in the nuclei (Fig. 4E and F), which is consistent with the results of previous studies (MacKay et al., 2009). Our data confirm a well-known fact, that free DOX permeates cellular and nuclear membranes by passive diffusion and tend to rapidly accumulate in the cell nuclei. Conversely, DOX loaded nanoparticles are expected to be taken up by cancer cells via endocytosis, followed by endosomal/lysosomal escape, drug release in the cytoplasm and subsequent drug diffusion to the nucleus. These processes are much slower than passive drug diffusion *in vitro* and would result in slow delivery of DOX encapsulated into IONPs to the cell nuclei (MacKay et al., 2009; Shi et al., 2009). Thus, cell uptake study revealed that after the same period of time (3 hrs) free DOX was internalized in A2780/AD cells two times more efficiently than DOX encapsulated in the developed delivery system (Fig. S7). In fact, this is one common reason why DOX delivered by nanocarriers usually have lower *in vitro* activity than the original molecular drug (MacKay et al., 2009; Shi et al., 2009). As expected, we observed that the encapsulation of DOX into IONPs decreased anticancer activity of the drug particularly at the higher concentrations (>1μg/mL) (Fig. 5A), supporting the differences in cellular internalization route and intracellular localization pattern. The half maximal inhibitory concentration ($IC_{50}$) for free DOX against A2780/AD was 1.9 μg/mL while this value for DOX loaded into the delivery system was 10.5 μg/mL, respectively. The detected cellular toxicity of free DOX against A2780/AD cell line is in a good agreement with previously published data, which revealed that $IC_{50}$ for free DOX against

A2780/AD cell line was ~ 4 μM (~ 2.1 μg/mL) (Savla et al., 2011). Thus, A2780/AD ovarian cancer cells were more sensitive to free DOX, which is likely due to free drug rapidly diffusing to the nucleus *in vitro*, whereas IONPs-DOX have to be trafficked through the cell before the drug is released and can reach the nucleus to intercalate DNA (MacKay et al., 2009). A similar behavior was previously described in the other studies, where DOX encapsulation in the nanoparticles-based delivery systems were less cytotoxic than free DOX under cell culture conditions due to longer time required for drug nuclear transportation (MacKay et al., 2009; Shi et al., 2009). Despite this behavior, the ultimate therapeutic outcome of DOX encapsulated in the delivery system is positive because the delivery system reduces the amount of available drug in the extracellular environment, and potentially diminishes unwanted side-target effects on healthy organs *in vivo* and inhibits multi drug resistance as compared to free DOX (MacKay et al., 2009). Therefore, another critical aspect for the development of an efficient drug delivery system is the ability of the drug to be predominantly released from the carrier in the cancer tumors and not in the blood stream. To assess the potential of the developed delivery system as a drug carrier capable of triggered drug release, the release profiles of DOX from IONPs-DOX-PEG-LHRH were evaluated at 37 °C in PBS buffer at pH 5.5 (pH of cancer tumor and endosomes) and 7.4 (pH of blood plasma) and human plasma (Hruby et al., 2005). The difference in release kinetics at pH 5.5 and 7.4 indicated that the pH strongly influenced DOX release from the developed drug delivery system, and the DOX release is more pronounced at pH 5.5 than at pH 7.4 (Fig. 5B). An initial burst release of 44.7% was detected within 2 hrs of IONPs-DOX-PEG-LHRH incubation at pH 5.5. Further incubation of the delivery system for 72 hrs under the same experimental conditions resulted in 91.1% of total drug release. In contrast, only 17.6% of the total DOX was gradually released at pH 7.4 after 72 hrs of incubation. A similar drug release pattern has been observed after incubation of the drug delivery system in 50% human plasma and resulted in 16.5% of total DOX release within 72 hrs. The obtained result is in good agreement with the previously published reports, which demonstrated that DOX exhibit pH dependent release from iron oxide nanoparticles modified with two polymer layers in tandem such as oleic acid and amphiphilic polymer containing carboxylic groups (Savla et al., 2011; Yang et al., 2008; Zou et al., 2010). There are two main reasons for the observed DOX behavior: (1) the protonation of the primary amine of DOX molecules under acidic pH which dramatically increased the solubility of the drug in an aqueous solution, and (2) the weakened interaction between DOX and the partially neutralized carboxyl groups of amphiphilic polymers under acidic pH (Zou et al., 2010). Such drug release behavior is important for an efficient and nontoxic drug delivery system because it ensures that there is low drug release at the physiological pH 7.4 during the transport of the drug in the blood stream, while there is fast or controlled drug release at acidic pH on arriving at the targeted tumor cells (Hruby et al., 2005; MacKay et al., 2009; Yang et al., 2008).

### 3.5 Heating properties of the delivery system: in vitro hyperthermia

Exposing iron oxide nanoparticles to AMF at a specified frequency can produce hyperthermia suitable for cancer treatment, and the efficiency of IONPs to generate heat is measured by the specific absorption rate (SAR) (Lee et al., 2011). Because the presence of coatings can compromise heating efficiencies of iron oxide nanoparticles, which in turn determine the efficacy of the treatment, the effect of drug loading and surface modification on the heat generation was evaluated based on SAR values of free IONPs and IONPs-DOX-PEG-LHR (Lee et al., 2011; Yuan et al., 2012). According to our data, loading with DOX and following coating with both PEG and LHRH layers did not significantly reduce the heating properties of the synthesized IONPs. The heating behavior of both non-modified IONPs and LHRH-PEG-DOX-IONPs of concentration 0.85 mg/mL subjected to AMF at the magnetic field frequency of 393 KHz and amplitude of 33.5 kA/m is shown in Figure 6A. The samples exhibited a similar heating rate reaching 50 °C in 7.5 min and 8.3 min for IONPs and IONPs-DOX-PEG-LHRH, respectively. The SAR values were calculated to be 289 W/g and 271 W/g for IONPs and PEG-LHRH-DOX-IONPs, respectively. The decrease in the SAR value for IONPs-DOX-PEG-LHRH is in good agreement with the magnetization study (Fig. S2B), which showed that drug loading and surface modification slightly decrease magnetic moments of IONPs. The obtained high SAR values indicate that the developed delivery system can be efficient for hyperthermia therapy.

To evaluate the suitability of the developed delivery system for hyperthermic applications we tested its capacity to generate heat intracellularly. For hyperthermia experiments cells were incubated with both drug free (IONPs-PEG-LHRH) and DOX loaded (IONPs-DOX-PEG-LHRH) delivery systems for 12 hrs at an iron concentration of 15μg/mL. This was followed by cells trypsinization, washing and centrifugation at a constant speed to form pellets consisting of 5 x $10^6$ cells. The cell pellets were placed in the coil to generate hyperthermia under exposure to AMF at constant magnetic field frequency of 393 kHz and maximum allowed amplitude of 33.5 kA/m. Our experimental design is based on previous studies that indicate that a maximum temperature change in a single cell transfected with iron oxide nanoparticles and exposed to AMF is negligible (Hedayati et al., 2012). Therefore, a collection of nanoparticle-containing cells into pellets would be necessary to achieve therapeutic levels of hyperthermia. Moreover, the hyperthermia generation efficiency also depends on the amount of iron oxide nanoparticles internalized by the cells (Hedayati et al., 2012). Thus, the amount of internalized iron in the cancer cells under these experimental conditions was quantified by using ferrozine assay as previously described (Basel et al., 2012). Both DOX loaded and drug free delivery systems entered cancer cells with similar efficiency, yielding a measured iron concentration of approximately 14.9 pg/cell and 11.1 pg/cell for IONPs-PEG-LHRH and IONPs-DOX-PEG-LHRH, respectively. After exposure of the formed cell pellets with the above mentioned nanoparticles loading to AMF, the maximum achieved temperature of cell pellets was as high as 44 °C. An example of a measured cell pellet temperature profile is represented in Figure 6B. Thus, with a starting temperature of 37 °C, the nanoparticles loaded A2780/AD cells exhibit rapid heating upon exposure to AMF, crossing 40 °C in 1.5 min and reaching 44 °C in 11.2 min. The achieved cellular temperature can be maintained during extended periods of time in the presence of AMF. However, switching off the AMF resulted in the rapid cooling of cells to 37 °C in 5 min. It appears realistic to heat remotely non accessible small tumors or disseminated metastases via intravenously injected tumor targeted IONPs.

The optimum temperature for most mild hyperthermia applications is in the 40–44 °C range (T<40 °C causes limited effect, T<44 °C results in thermoablation), and requires durations of 30–60 min (Falk and Issels, 2001; Levi-Polyachenko and Stewart, 2011). Therefore, our hyperthermia treatment experiments were performed at two different temperatures, 40 ºC and 44 °C, with an exposure period of 30 min. These two temperatures were specifically selected to evaluate the cytotoxicity effects of mild hyperthermia on A2780/AD ovarian cancer cells at the accepted lower and upper temperatures. The desired cellular temperatures were achieved by varying magnetic field amplitude at a constant magnetic field frequency of 393 kHz. Thus, exposure of A2780/AD cells transfected with IONPs-PEG-LHRH to AMF with field amplitude of 33.5 kA/m resulted in the maximum temperature of 44 °C, while decreasing field amplitude to 21.2 kA/m lowered cellular temperature to 40 ºC. Subsequently, the treated cells were seeded in

96 well plates and viability was analyzed 48 hrs after hyperthermia treatment in order to investigate whether mild hyperthermia promoted apoptosis on drug resistant ovarian cancer cells. The effects of hyperthermia treatments on the cell viability, at two temperatures (40 ºC and 44 ºC), can be seen in Figure 7. The results indicated that cell viability decreased by 95% at 44 °C (Fig.7, bar 4), while mild hyperthermia at a lower temperature (40 °C) was less efficient resulting in a 72% reduction of cellular viability (Fig.7, bar 5). Experimental controls performed on cell viability demonstrated that neither IONPs alone (Fig.7, bar 3) nor the applied magnetic field (Fig.7, bar 2) effected cell viability under the studied experimental conditions. Therefore, heat generated by the developed delivery system is the main mechanism for the cell death under an AMF.

### 3.6 Combinatorial treatment

Numerous studies have demonstrated that the combination of mild hyperthermia with a number of conventional chemotherapeutic agents at lower therapeutic dosages result in additive or synergistic therapeutic effects (Kulshrestha et al., 2012; Pradhan et al., 2010). Therefore, the main goal of this work was not to kill the cancer cells with higher concentrations of either anticancer drug or high temperature, but rather to demonstrate an efficacy of the combinatorial treatment achieved with the developed delivery system at lower therapeutic doses of mild hyperthermia and chemotherapeutic agent. Consequently, the concentrations of 1μg/mL of DOX and 15 μg/mL of IONPs incorporated in the tumor targeted delivery system were employed for the current study. Our choice was based on the fact that the selected DOX concentration alone cannot significantly enhance cell apoptosis and leaves over 70% of the cells viable after treatment (Fig. 5A and Fig. 7, bar 6). Further, the employed concentration of IONPs is not toxic to A2780 cells (Fig. 15A, Fig. S3B and Fig. 8, bar 3) and results in substantial cellular heat generation required for mild hyperthermia conditions (40-44 °C) under exposure to AMF (Fig. 6B). Because 44 °C is lethal to the cancer cells under the studied conditions (viability of the cells decreased over 95%), the lowest temperature accepted for mild hyperthermia (40 °C) was chosen for the combinatorial treatment experiment and was attained by adjusting field amplitude to 21.2 kA/m. Our data demonstrated that the combination of the chemotherapeutic drug and mild hyperthermia resulted in over 95% cell death (Fig.7, bar 7), while either chemotherapy alone (Fig.7, bar 6) or nanoparticles-mediated mild hyperthermia (Fig.7, bar 5) decreased cell viability by 27% and 72%, respectively. It can be concluded that the cytotoxic effect of the combinatorial treatment achieved with the developed delivery system is superior to each of the two treatments applied separately, and an evaluation using Valeriote's formula (Pradhan et al., 2010) showed that the combined effects were synergistic in nature. Obviously, the developed delivery system can be efficiently used for killing of ovarian cancer cells by only hyperthermia (Fig. 7, bar 4) at the higher temperature (44 °C). However, to avoid damage to surrounding healthy tissue, it is highly desirable to keep the local temperature during hyperthermia treatment under 44 °C and whole body temperatures less than 42 °C, which is the upper limit compatible with life. Thus, an advantage of the proposed combinatorial treatment approach is based on the concurrent application of two treatment modalities at their respective safe doses that work by different mechanisms, thereby increasing tumor cell killing while minimizing overlapping toxicity to healthy organs.

## 4. Conclusions

We have successfully synthesized and tested a tumor-targeting multifunctional delivery system for combinatorial treatment of ovarian cancer. The developed nanocarriers have a hydrodynamic diameter less than 100 nm and a zeta potential close to zero, which make them stable in biological media and decreases their elimination by the immune system. The developed delivery system demonstrated low cytotoxicity and high efficiency in the delivery of DOX, and mild hyperthermia to drug resistant ovarian cancer cells. The prepared nanocarriers are capable of drug triggered release in an acidic environment and, therefore, DOX can be predominantly dissociated from IONPs within a cancer tumor, but not during the systemic circulation after intravenous administration. Due to superparamagnetic behavior of the developed IONPs, the delivery system can efficiently heat cancer cells remotely upon exposure to AMF and the desired temperature can be achieved by varying magnetic field strength. Moreover, lower doses of chemotherapeutic drug and mild hyperthermia delivered by the developed nanocarrier synergistically decreased viability of drug resistant ovarian cancer cells. Thus, much higher therapeutic outcomes with fewer side effects can be reached with combinatorial treatment of ovarian cancer by employing lower doses of chemotherapeutic drugs and mild hyperthermia incorporated in the developed delivery system.

**Acknowledgements**

This work was supported in part by funding provided by the Medical Research Foundation of Oregon, PhRMA Foundation and the College of Pharmacy, Oregon State University. We thank Dr. Brian Dolan and Amy L. Palmer from the College of Veterinary Medicine, OSU for their help with flow cytometry analysis. The funding sources had no involvement in the study design; in the collection, analysis and interpretation of data; in the writing of the report; or in the decision to submit the article for publication.

**Appendix A. Supplementary data**

## References


Ahmd, M., Rashid, K., Nadeem, M., Masood, K., Ali, S., Nafees, M., Gull, N., Mumtaz-ul-Haq, Ibrahim, N., Saeed, A., Qureshy, A., Aleem, F., Naseer, H., Mehmood, S., Hyder, S.W., 2012. A simple method to prepare aqueous dispersion of iron oxide nanoparticles and their biodistribution study J. Colloid Sci. Biotechnol. 1, 201-201.

Ahsan, A., Aziz, A., Arshad, M.A., Ali, O., Nauman, M., Ahmad, N.M., Elaissari, A., 2013. Smart magnetically engineering colloids and biothin films for diagnostics applications. J. Colloid Sci. Biotechnol. 2, 19-26.

Alexis, F., Pridgen, E., Molnar, L.K., Farokhzad, O.C., 2008. Factors affecting the clearance and biodistribution of polymeric nanoparticles. Mol. Pharmaceut. 5, 505-515.

Basel, M.T., Balivada, S., Wang, H.W., Shrestha, T.B., Seo, G.M., Pyle, M., Abayaweera, G., Dani, R., Koper, O.B., Tamura, M., Chikan, V., Bossmann, S.H., Troyer, D.L., 2012. Cell-delivered magnetic nanoparticles caused hyperthermia-mediated increased survival in a murine pancreatic cancer model. Int. J. Nanomedicine 7, 297-306.

Falk, M.H., Issels, R.D., 2001. Hyperthermia in oncology. Int. J. Hyperthermia 17, 1-18.

Fan, C.X., Gao, W.H., Chen, Z.X., Fan, H.Y., Lie, M.Y., Deng, F.J., Chen, Z.L., 2011. Tumor selectivity of stealth multi-functionalized superparamagnetic iron oxide nanoparticles. Int. J. Pharmaceut. 404, 180-190.

Fortin, J.P., Wilhelm, C., Servais, J., Menager, C., Bacri, J.C., Gazeau, F., 2007. Size-sorted anionic iron oxide nanomagnets as colloidal mediators for magnetic hyperthermia. J. Am. Chem. Soc. 129, 2628-2635.

Gou, P.F., Zhu, W.P., Shen, Z.Q., 2010. Synthesis, self-assembly, and drug-loading capacity of well-defined cyclodextrin-centered drug-conjugated amphiphilic A(14)B(7) miktoarm star copolymers based on poly(epsilon-caprolactone) and poly(ethylene glycol). Biomacromolecules 11, 934-943.

Hedayati, M., Thomas, O., Abubaker-Sharif, B., Zhou, H., Cornejo, C., Zhang, Y., Wabler, M., Mihalic, J., Gruettner, C., Westphal, F., Geyh, A., Deweese, T.L., Ivkov, R., 2012. The effect of cell cluster size on intracellular nanoparticle-mediated hyperthermia: is it possible to treat microscopic tumors? Nanomedicine (Lond) 8, 29-41.

Hruby, M., Konak, C., Ulbrich, K., 2005. Polymeric micellar pH-sensitive drug delivery system for doxorubicin. J. Control. Release 103, 137-148.

Jelovac, D., Armstrong, D.K., 2011. Recent progress in the diagnosis and treatment of ovarian cancer. CA Cancer J. Clin. 61, 183-203.

Kievit, F.M., Wang, F.Y., Fang, C., Mok, H., Wang, K., Silber, J.R., Ellenbogen, R.G., Zhang, M.Q., 2011. Doxorubicin loaded iron oxide nanoparticles overcome multidrug resistance in cancer in vitro. J. Control. Release 152, 76-83.

Kleef, R., Kekic, S., Ludwig, N., 2012. Successful treatment of advanced ovarian cancer with thermochemotherapy and adjuvant immune therapy. Case Rep. Oncol. 5, 212–215.

Kulshrestha, P., Gogoi, M., Bahadur, D., Banerjee, R., 2012. In vitro application of paclitaxel loaded magnetoliposomes for combined chemotherapy and hyperthermia. Colloid. Surface B 96, 1-7.

Lee, J.H., Jang, J.T., Choi, J.S., Moon, S.H., Noh, S.H., Kim, J.W., Kim, J.G., Kim, I.S., Park, K.I., Cheon, J., 2011. Exchange-coupled magnetic nanoparticles for efficient heat induction. Nat. Nanotechnol. 6, 418-422.

Lengyel, E., 2012. Ovarian cancer development and metastasis. Am. J. Pathol. 177, 1053-1064.

Levi-Polyachenko, N.H., Stewart, J.H., 2011. Clinical relevance of nanoparticle induced hyperthermia for drug delivery and treatment of abdominal cancers. Open Nanomedicine J. 3, 24-37.

Longmire, M., Choyke, P.L., Kobayashi, H., 2008. Clearance properties of nano-sized particles and molecules as imaging agents: considerations and caveats. Nanomedicine-UK 3, 703-717.

MacKay, J.A., Chen, M.N., McDaniel, J.R., Liu, W.G., Simnick, A.J., Chilkoti, A., 2009. Self-assembling chimeric polypeptide-doxorubicin conjugate nanoparticles that abolish tumours after a single injection. Nat. Mater. 8, 993-999.

Maruyama, K., 2011. Intracellular targeting delivery of liposomal drugs to solid tumors based on EPR effects. Adv. Drug Deliver. Rev. 63, 161-169.

Moros, M., Pelaz, B., Lopez-Larrubia, P., Garcia-Martin, M.L., Grazu, V., de la Fuente, J.M., 2010. Engineering biofunctional magnetic nanoparticles for biotechnological applications. Nanoscale 2, 1746-1755.

Peng, X.H., Qian, X.M., Mao, H., Wang, A.Y., Chen, Z., Nie, S.M., Shin, D.M., 2008. Targeted magnetic iron oxide nanoparticles for tumor imaging and therapy. Int. J. Nanomedicine 3, 311-321.

Pradhan, P., Giri, J., Rieken, F., Koch, C., Mykhaylyk, O., Doblinger, M., Banerjee, R., Bahadur, D., Plank, C., 2010. Targeted temperature sensitive magnetic liposomes for thermo-chemotherapy. J. Control. Release 142, 108-121.

Quan, Q.M., Xie, J., Gao, H.K., Yang, M., Zhang, F., Liu, G., Lin, X., Wang, A., Eden, H.S., Lee, S., Zhang, G.X., Chen, X.Y., 2011. HSA coated iron oxide nanoparticles as drug delivery vehicles for cancer therapy. Mol. Pharmaceut. 8, 1669-1676.

Savla, R., Taratula, O., Garbuzenko, O., Minko, T., 2011. Tumor targeted quantum dot-mucin 1 aptamer-doxorubicin conjugate for imaging and treatment of cancer. J. Control. Release 153, 16-22.

Sehouli, J., Stengel, D., Oskay-Oezcelik, G., Zeimet, A.G., Sommer, H., Klare, P., Stauch, M., Paulenz, A., Camara, O., Keil, E., Lichtenegger, W., 2008. Nonplatinum topotecan combinations versus topotecan alone for recurrent ovarian cancer: results of a phase III study of the North-Eastern German Society of Gynecological Oncology Ovarian Cancer Study Group. J. Clin. Oncol. 26, 3176-3182.

Shi, M., Ho, K., Keating, A., Shoichet, M.S., 2009. Doxorubicin-conjugated immuno-nanoparticles for intracellular anticancer drug delivery. Adv. Funct. Mater. 19, 1689-1696.

Taratula, O., Garbuzenko, O.B., Chen, A.M., Minko, T., 2011a. Innovative strategy for treatment of lung cancer: targeted nanotechnology-based inhalation co-delivery of anticancer drugs and siRNA. J. Drug Target. 19, 900-914.

Taratula, O., Garbuzenko, O.B., Kirkpatrick, P., Pandya, I., Savla, R., Pozharov, V.P., He, H.X., Minko, T., 2009. Surface-engineered targeted PPI dendrimer for efficient intracellular and intratumoral siRNA delivery. J. Control. Release 140, 284-293.

Taratula, O., Garbuzenko, O.B., Savla, R., Wang, Y.A., He, H., Minko, T., 2011b. Multifunctional nanomedicine platform for cancer specific delivery of siRNA by superparamagnetic iron oxide nanoparticles-dendrimer complexes. Curr. Drug Deliv. 8, 59-69.

Wang, L., Zhang, J., An, Y.L., Wang, Z.Y., Liu, J., Li, Y.T., Zhang, D.S., 2011. A study on the thermochemotherapy effect of nanosized $As_2O_3$/MZF thermosensitive magnetoliposomes on experimental hepatoma in vitro and in vivo. Nanotechnology 22, 315102.

Yang, L.L., Cao, Z.H., Sajja, H.K., Mao, H., Wang, L.Y., Geng, H.Y., Xu, H.Y., Jiang, T.S., Wood, W.C., Nie, S.M., Wang, Y.A., 2008. Development of receptor targeted magnetic iron oxide nanoparticles for efficient drug delivery and tumor imaging. J. Biomed. Nanotechnol. 4, 439-449.

Yang, L.L., Peng, X.H., Wang, Y.A., Wang, X.X., Cao, Z.H., Ni, C.C., Karna, P., Zhang, X.J., Wood, W.C., Gao, X.H., Nie, S.M., Mao, H., 2009. Receptor-targeted nanoparticles for in vivo imaging of breast cancer. Clin. Cancer Res. 15, 4722-4732.

Yang, X.Q., Grailer, J.J., Rowland, I.J., Javadi, A., Hurley, S.A., Matson, V.Z., Steeber, D.A., Gong, S.Q., 2010. Multifunctional stable and pH-responsive polymer vesicles formed by heterofunctional triblock copolymer for targeted anticancer drug delivery and ultrasensitive MR imaging. ACS Nano 4, 6805-6817.

Yezhelyev, M.V., Qi, L.F., O'Regan, R.M., Nie, S., Gao, X.H., 2008. Proton-sponge coated quantum dots for siRNA delivery and intracellular imaging. J. Am. Chem. Soc. 130, 9006-9012.

Yu, M.K., Park, J., Jon, S., 2012a. Targeting strategies for multifunctional nanoparticles in cancer imaging and therapy. Theranostics 2, 3-44.

Yu, S.S., Lau, C.M., Thomas, S.N., Jerome, W.G., Maron, D.J., Dickerson, J.H., Hubbell, J.A., Giorgio, T.D., 2012b. Size- and charge-dependent non-specific uptake of PEGylated nanoparticles by macrophages. Int. J. Nanomedicine 7, 799-813.

Yu, W.W., Chang, E., Sayes, C.M., Drezek, R., Colvin, V.L., 2006. Aqueous dispersion of monodisperse magnetic iron oxide nanocrystals through phase transfer. Nanotechnology 17, 4483-4487.

Yuan, Y., Rende, D., Altan, C.L., Bucak, S., Ozisik, R., Borca-Tasciuc, D.A., 2012. Effect of surface modification on magnetization of iron oxide nanoparticle colloids. Langmuir 28, 13051-13059.

Zhang, M., Garbuzenko, O.B., Reuhl, K.R., Rodriguez-Rodriguez, L., Minko, T., 2012. Two-in-one: combined targeted chemo and gene therapy for tumor suppression and prevention of metastases. Nanomedicine-UK 7, 185-197.

Zhang, Y., Kohler, N., Zhang, M.Q., 2002. Surface modification of superparamagnetic magnetite nanoparticles and their intracellular uptake. Biomaterials 23, 1553-1561.

Zou, P., Yu, Y.K., Wang, Y.A., Zhong, Y.Q., Welton, A., Galban, C., Wang, S.M., Sun, D.X., 2010. Superparamagnetic iron oxide nanotheranostics for targeted cancer cell imaging and pH-dependent intracellular drug release. Mol. Pharmaceut. 7, 1974-1984.

## Figure Legends

**Figure 1.** Surface-engineered approach for preparation of iron oxide nanoparticle (IONPs)-based nanocarrier for a targeted co-delivery of anticancer drug and heat. (A) Loading of anticancer agent (DOX) into the polymer reservoir on IONPs surface. (B) Surface modification of DOX-loaded IONPs with PEG. (C) Conjugation of LHRH peptide to the distal end of PEG.

**Figure 2.** TEM images and size distribution histograms of (A, B) iron oxide nanoparticles (IONPs) and (C, D) DOX loaded nanoparticles modified with PEG and LHRH peptide (IONPs-DOX-PEG-LHRH).

**Figure 3.** Representative fluorescence microscopy images of A2780/AD cancer cells incubated for 10 hrs with (A, B) DOX loaded iron oxide nanoparticles (IONPs-DOX), (C, D) IONPs-DOX modified with PEG (IONPs-DOX-PEG) and (E, F) IONPs-DOX modified with both PEG and LHRH peptide (IONPs-DOX-PEG-LHRH). A, C and E represent light images of A2780/AD cells; B, D and F represent fluorescent images of DOX delivered into A2780/AD cells by IONPs with different modifications. The fluorescent images were taken with the same exposure times to allow comparisons of DOX internalization efficiency delivered by different systems. The red arrows indicate strong aggregation of non-modified DOX loaded iron oxide nanoparticles (IONPs-DOX) in cell culture medium containing 10% of fetal bovine serum.

**Figure 4.** Intracellular localization of DOX in A2780/AD cancer cells after incubation with LHRH targeted drug delivery systems (IONPs-DOX-PEG-LHRH) for (A, B) 3 hrs and (C, D) 24 hrs and free DOX for 3 hrs (E, F) followed by DAPI staining. A, C and E represent light images

of A2780/AD cells; B, D and F represent superimposed fluorescence images of DAPI stained nuclei (blue color) and DOX (red color). Superimposition of fluorescence images allows for detecting of nuclear localization of DOX resulting in purple color.

**Figure 5.** (A) *In vitro* cytotoxicity of free DOX, DOX loaded into IONPs-based drug delivery system (IONPs-DOX-PEG-LHRH) and DOX-free drug delivery system (IONPs-PEG-LHRH) against A2780/AD human ovarian cancer cells after 24 hrs of incubation. (B) The release profiles of DOX from IONPs-DOX-PEG-LHRH incubated at 37 °C in 50% of human plasma and PBS buffer at pH 5.5 and pH 7.4.

**Figure 6.** (A) Heating profiles of non-modified IONPs and IONPs-DOX-PEG-LHRH of concentration 0.85 mg/mL subjected to AMF at magnetic field frequency of 393 KHz and amplitude of 33.5 kA/m. (B) Dynamic temperature profile of A2780/AD cells transfected with IONPs-PEG-LHRH (Fe concentration- 15 μg/mL) and exposed to AMF (33.5 kA/m and 393 kHz). Cells were allowed to equilibrate to 37 °C in the sample chamber for 7 min before AMF was turned on. The arrows indicate when AMF was turned on and off, respectively.

**Figure 7.** Viability of A2780/AD ovarian cancer cells after treatment with the following formulations (1) control (no treatment), (2) exposure to AMF only (33.5 kA/m and 393 kHz), (3) IONPs-PEG-LHRH (Fe concentration- 15 μg/mL), (4) 44 °C hyperthermia for 30 min: cells were incubated with IONPs-PEG-LHRH (Fe concentration- 15 μg/mL) and exposed to AMF (33.5 kA/m and 398 kHz), (5) 40 °C hyperthermia for 30 min: cells were incubated with IONPs-PEG-LHRH (Fe concentration- 15 μg/mL) and exposed to AMF (21.2 kA/m and 393 kHz), (6)

chemotherapy: cells were treated with IONPS-DOX-PEG-LHRH (Fe concentration- 15 μg/mL, DOX concentration- 1 μg/mL) and (7) combinatorial treatment: chemotherapy (DOX concentration- 1 μg/mL) and hyperthermia (40 °C for 30 min). Cells were incubated with IONPs-DOX-PEG-LHRH and exposed to AMF (21.2 kA/m and 398 kHz).

| Formulations | Size (nm)[a] | Size (nm)[b] | PDI[b] | Zeta potential (mV) |
|---|---|---|---|---|
| IONPs | 34.2 ± 2.1 | 70.8 ± 0.2 | 0.141 ± 0.010 | +38.0 ± 1.8 |
| IONPs-DOX | 37.5 ± 2.1 | 86.4 ± 0.7 | 0.129 ± 0.012 | +42.6 ± 0.7 |
| IONPs-DOX-PEG-LHRH | 43.5 ± 2.8 | 97.1 ± 1.0 | 0.218 ± 0.037 | +4.9 ± 0.9 |

**Table 1.** Physicochemical characterization of iron oxide nanoparticle-based formulations

[a] TEM measurements [b] DLS measurements

*Graphical Abstract (for review)

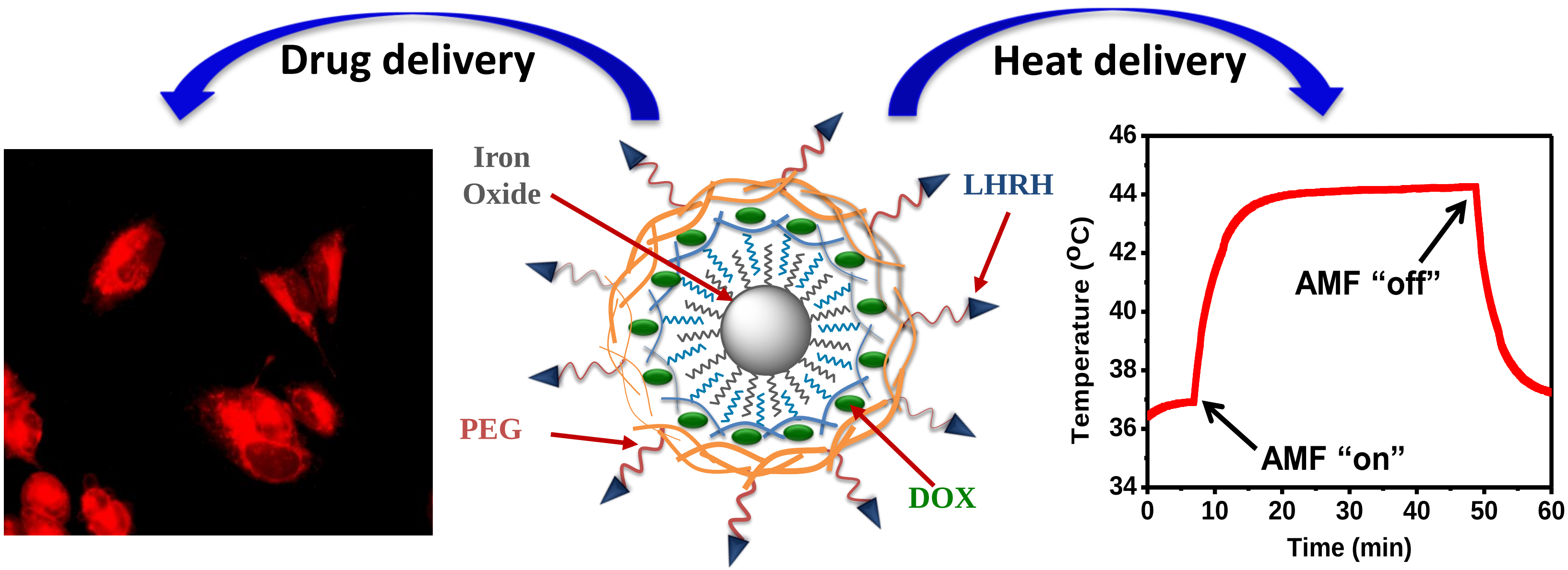


Nanocarrier for concurrent delivery of chemotherapeutic drug and heat

Figure 1

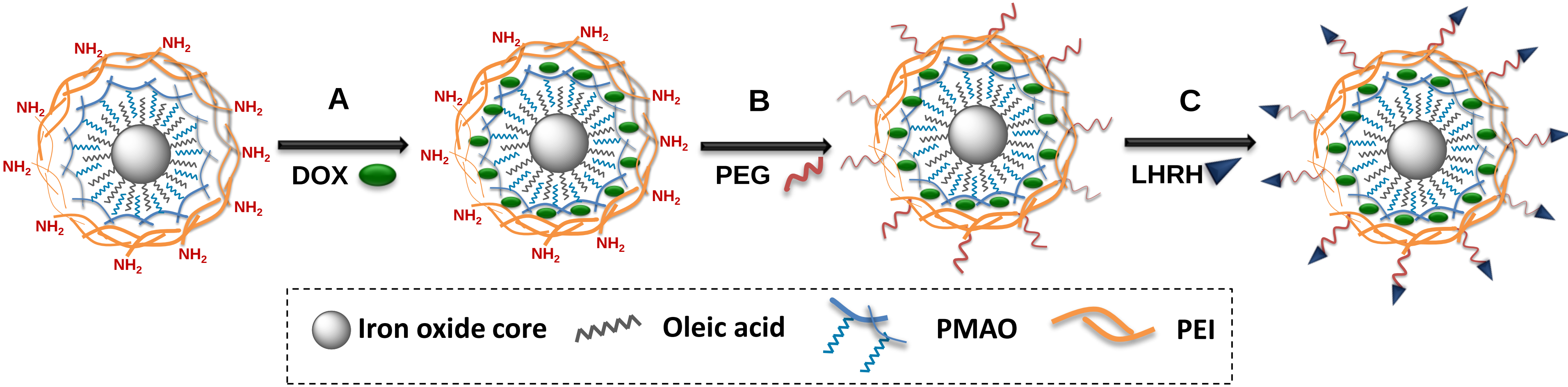

Figure 2

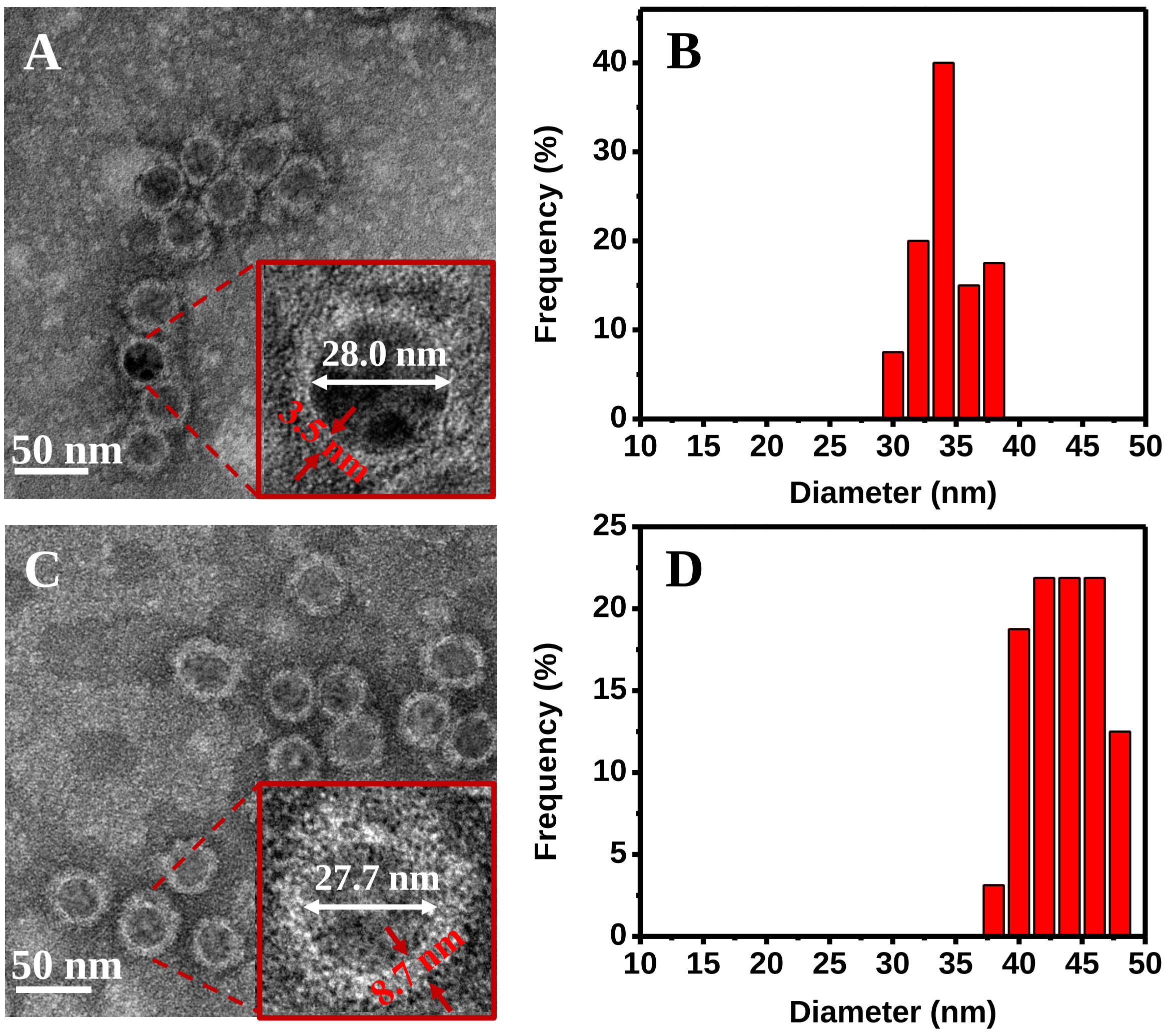
A
28.0 nm
3.5 nm
50 nm
B
Frequency (%)
Diameter (nm)
C
27.7 nm
8.7 nm
50 nm
D
Frequency (%)
Diameter (nm)

**Figure 3**

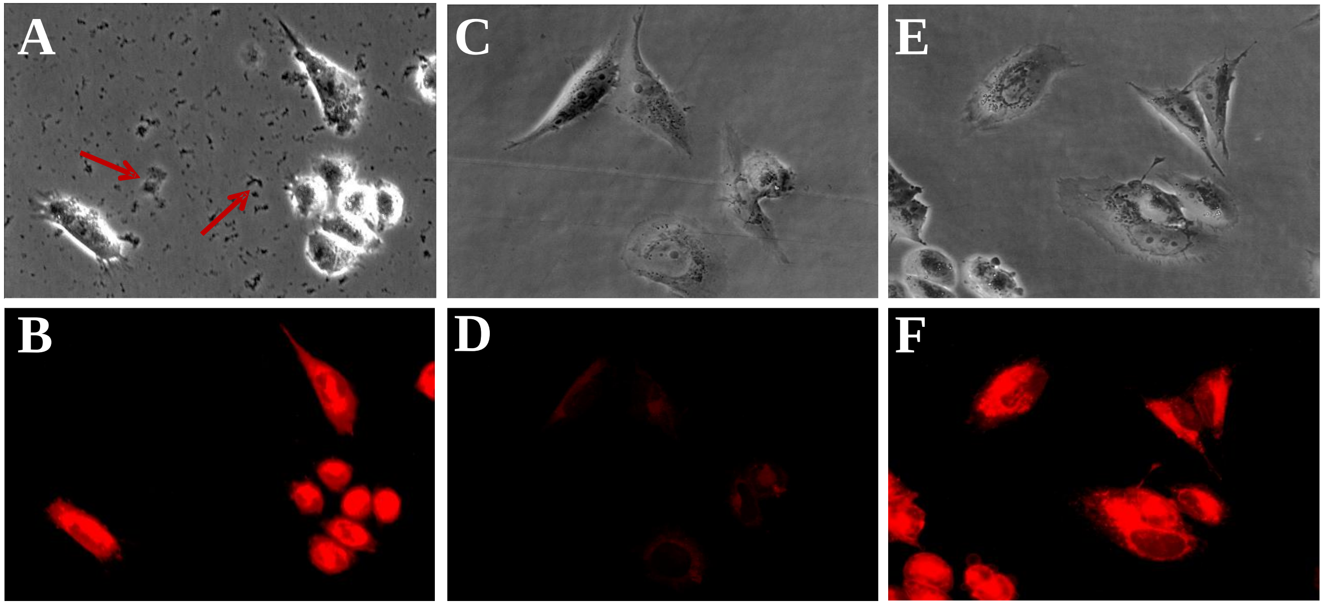

Figure 4

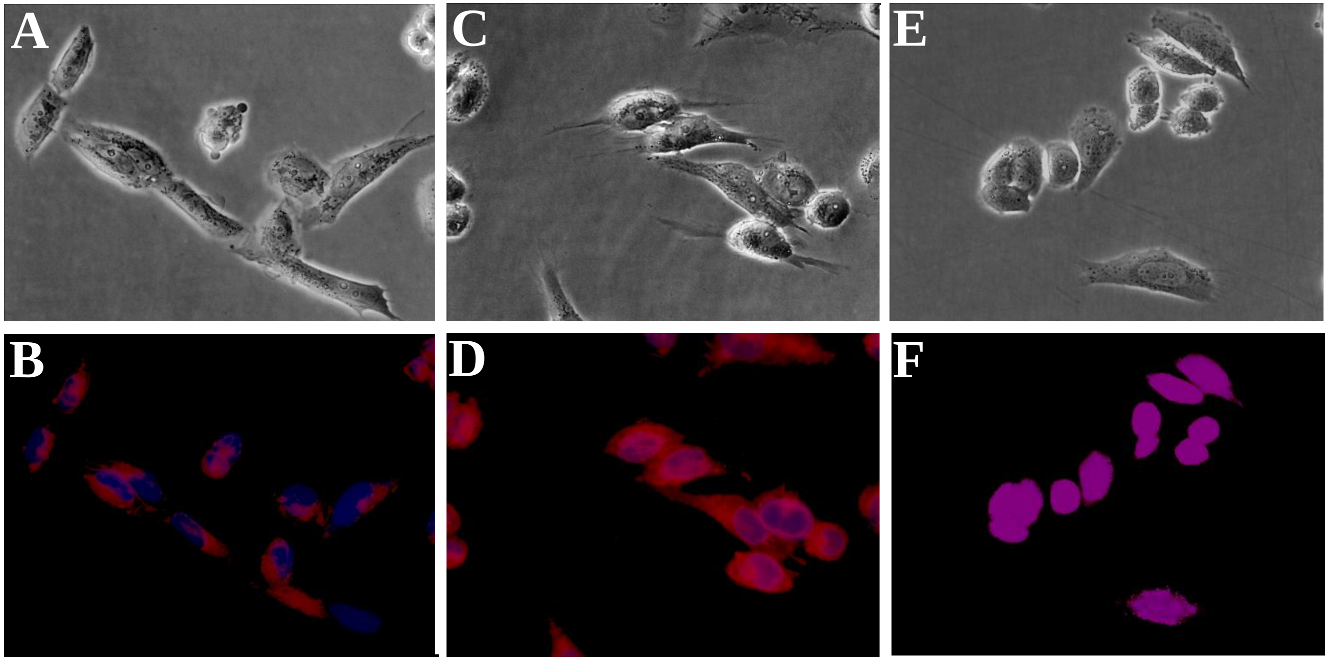

**Figure 5**

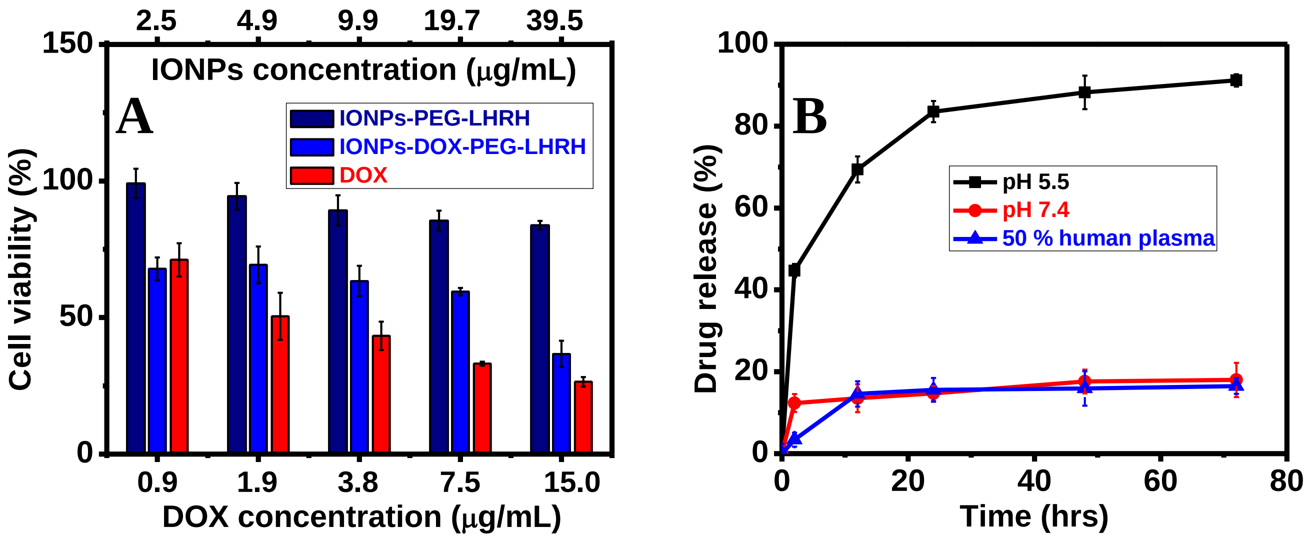

2.5
4.9
9.9
19.7
39.5
150
IONPs concentration (μg/mL)
A
IONPs-PEG-LHRH
IONPs-DOX-PEG-LHRH
DOX
100
50
0
Cell viability (%)
0.9
1.9
3.8
7.5
15.0
DOX concentration (μg/mL)
100
B
80
60
40
20
0
Drug release (%)
pH 5.5
pH 7.4
50 % human plasma
0
20
40
60
80
Time (hrs)

Figure 6

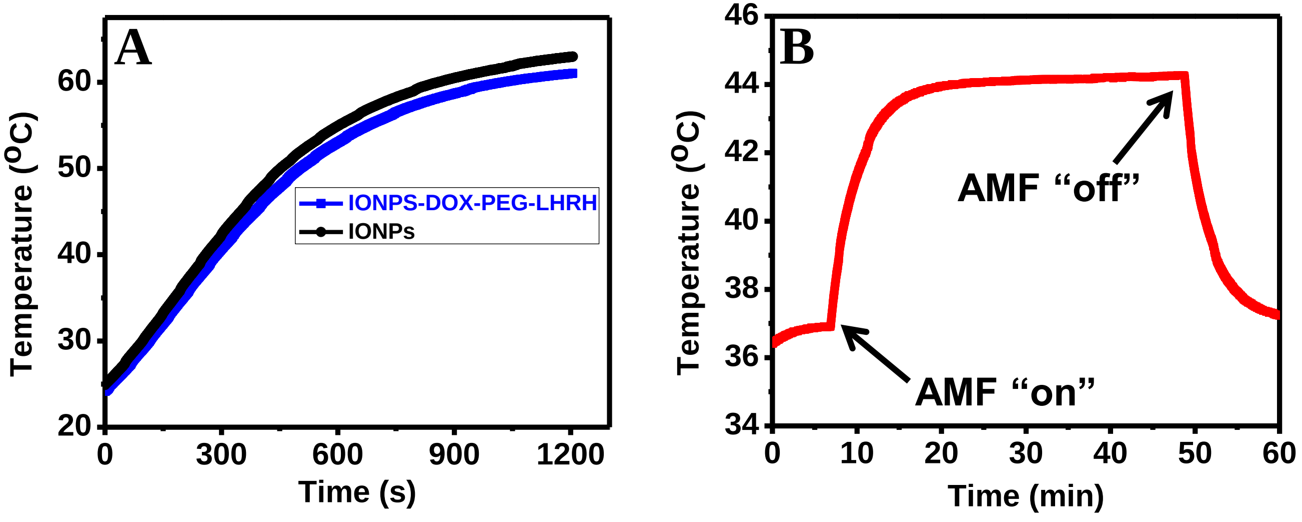
A
Temperature (oC)
Time (s)
IONPS-DOX-PEG-LHRH
IONPs
20
30
40
50
60
0
300
600
900
1200
B
Temperature (oC)
Time (min)
AMF “off”
AMF “on”
34
36
38
40
42
44
46
0
10
20
30
40
50
60

**Figure 7**